Water Science & Technology

IWA PUBLISHING

Water Science & Technology Vol 85 No 4, 1040 doi: 10.2166/wst.2021.637

UV-light-driven cadmium sulphide (CdS) nanocatalysts: synthesis, characterization, therapeutic and environmental applications; kinetics and thermodynamic study of photocatalytic degradation of Eosin B and Methyl Green dyes

Sundas Ali[a], F. Akbar Jan[a,*], Rahat Ullah[a], Wajidullah[a], Naimat Ullah[b] and Salman[c]

[a] Department of Chemistry, Bacha Khan University Chrasadda, Khyber-Pakhtunkhwa 24420, Pakistan
[b] Department of Chemistry, Qauid-i-Azam University Islamabad, Islamabad 45320, Pakistan
[c] Department of Biotechnology, Bacha Khan University Chrasadda, Khyber-Pakhtunkhwa 24420, Pakistan
*Corresponding author. E-mail: fazal_akbarchem@yahoo.com

FA-J, 0000-0001-9210-4664

ABSTRACT

Cadmium sulphide (CdS) nanoparticles (NPs) were synthesized through hydrothermal route and characterized by UV-Vis spectroscopy, X-ray diffraction (XRD), Energy dispersive X-ray analysis, Scanning electron microscopy (SEM), Fourier transform infrared spectroscopy and Thermo gravimetric analysis (TGA).The band gap of CdS nanoparticles was found to be 2.38 eV. CdS NPs are crystalline aggregates with hexagonal structure as shown by SEM and XRD analysis. TGA study revealed that the synthesized nanomaterials were very stable to temperature and only 6.54% total loss occurred during heating range (25 °C–600 °C).The CdS NPs were used for the first time against the degradation of Eosin B (EB) and Methyl green (MG) dyes in aqueous solution.The degradation of EB and MG over CdS nanocatalysts followed second order kinetics. The predicted activation energies for both the dyes' reactions were 61.1 kJ/mol and 32.11 kJ/mol, respectively. About 95% and 90% dye degradation was observed at the time interval of 160 minutes for EB and MG, respectively. High percent degradation of EB was observed at high pH (pH 0) while at low pH (pH 4) high percent degradation was found for MG dye. Maximum dye degradation was found at the optimal dose (0.03 g/L) of the catalyst and at low dye concentration. The rate of EB and MG dye degradation was found to increase with increase in temperature up to 45 °C. The recyclability study showed that CdS nanoparticles could be reused for the degradation of the given dyes. Good antibacterial activity against *Staphylococcus aureus* was shown by CdS NPs. From the biocompatibility it was confirmed that CdS NPS are bioincompatible compatible.

Key words: biological assays, cadmium sulphide nanoparticles, Eosin B, kinetic and thermodynamic study, Methyl Green, recycled catalyst

HIGHLIGHTS

- The band gap was 2.38 eV.
- Dyes degradation over followed second order kinetics.
- 61.1 kJ/mol and 32.11 kJ/mol were activation energies.
- 95% and 90% dye degradation was observed for EB and MG, respectively.
- Good antibacterial activity against *Staphylococcus aureus*.
- CdS NPS were found bioincompatible compatible.

INTRODUCTION

Industrial effluents containing dyes pose a serious environmental hazard since their dumping into natural water bodies frequently results in environmental contamination, functioning as a source of non-aesthetic pollution, eutrophication, and so causing harm to aquatic life. The removal or degradation of stubborn synthetic dyes is a major ecological issue that is difficult to solve. For the removal of synthetic colourants from wastewater, several methods such as electrolysis, adsorption, oxidation, coagulation, active sludge biochemical processes, membrane filtering, ozonization, and bio-degradation have been utilized (Menon *et al.* 2021). Advanced oxidation processes (AOPs), a promising technique, have recently been widely used for decolorization and degradation of textile dyes. The heterogeneous photocatalytic oxidation method is a technology that uses

photocatalysts that is currently being investigated (Sarkar *et al.* 2020). Photocatalysts may degrade a variety of organic contaminants and pigments. To activate the photo-induced electrons, they need light energy. The charge carrier recombines to create H_2O molecules when photo-generated electrons from the valence band (VB) are transported to conduction band (CB). Meanwhile, in the VB, H_2O molecules are oxidized to enhance the quantity of •OH generated, which is used to destroy the synthetic colours. In photo oxidation, organic contaminants are completely oxidized in a short interval of time. Furthermore, no additional hazardous compounds are formed during this procedure (Lee *et al.* 2020).

Cadmium sulphide (CdS) nanoparticles have piqued interest among various nanoparticles due to the availability of discrete energy levels, size dependent optical properties, and a tunable bandgap, as well as a well-developed synthetic protocol, easy preparation technique, and good chemical stability (Desai *et al.* 2017). Due to the high photosensitivity of CdS, it is utilized in the detection of visible radiations, light emitting diodes, solar cells, photochemical catalysis, gas sensors, other luminescence devices, optoelectronic devices, and a range of biological applications (Blažeka *et al.* 2020; Chang *et al.* 2020; Mullamuri *et al.* 2021).

Pharmaceutical contaminants and bacteria have also been a source of concern, as they are absorbed by various water streams via wastewater effluents, industrial and agricultural operations (Munyai *et al.* 2021). For this purpose CdS nanoparticles were tested against *Escherichia coli, Bacillus licheniformis, Pseudomonas aeruginosa*, *Staphylococcus aureus*, and *B. cereus* at a dosage of 40 mg/mL CdS (Rajeshkumar *et al.* 2014), taking into account that CdS semiconductors can behave as photocatalysts in the photodegradation of the environmental organic pollutants and as antibacterial agents.

The benefits of the photocatalysis were kept in mind and a study was designed to synthesize and characterize CdS nanoparticles and to apply as a catalyst for the photo degradation of MG and EB dyes in aqueous medium. Investigation of order of reaction of photocatalytic degradation of selected dyes using CdS nanocatalyst was also the objective of the present study. Therapeutic applications of CdS NPs were among the aims of the study.

EXPERIMENTAL

Apparatus

UV-visible spectrophotometer (Model Shimadzu UV-1800), Perkin Elmer Fourier transform infrared (FTIR) spectrometer version 10.4.00, TGA (Shimadzu TGA -50/50H) were used for characterization and analysis of the synthesized materials in Advance Research Lab (ARL) Department of Chemistry Bacha Khan University Chrasadda. Synthesized materials were also characterized using X-ray diffraction (XRD), scanning electron microscopy (SEM) and energy dispersive X-ray (EDX) in Quaid-i-Azam University Islamabad.

Synthesis of CdS nanoparticles

CdS NPs were synthesized through hydrothermal route. In this typical synthesis 15 mL (0.1 M) of each Cd $(NO_3)_2.4H_2O$ and $Na_2S.9H_2O$ solutions were taken in a beaker. The mixed solution was stirred at room temperature for about 10 minutes. Then the mixture was transferred to 50 mL autoclave and was placed in a muffle furnace for 14 hours at 200 °C. After heating the reaction mixture, it was centrifuged and washed four times with water. The final product was dried at 50 °C for five hours (Supplementary Figure 1).

Preparation of the dye solution

Stock solutions (500 ppm) of EB and MG dyes were prepared separately in distilled water. Using dilution formula given in Equation (1), the working solutions of different concentration were prepared accordingly.

$$M_1V_1 = M_2V_2 \quad (1)$$

Photocatalytic degradation of the dyes

The activity of CdS nanoparticles was evaluated while using them for the degradation of EB and MG dyes in aqueous solution. The degradation was carried out in UV-light. The λ_{max} of EB and MG was found at 516 nm and 645 nm and was used as monitor wavelengths. Upon addition of an appropriate amount of photocatalyst (CdS, NPs) the dye solution was stirred for 20 minutes in the dark to establish adsorption/desorption equilibrium. Light source was placed 15 cm away from the surface of the solution during experiments in locally designed equipment. The catalyst was removed by centrifugation and the dye degradation was checked at various intervals of time using UV-Visible spectrophotometer. The same process was

repeated in sun-light. The following relation (Equation (2)) was used to calculate percent degradation of the dye.

$$D\ (\%) = \frac{C_o - C}{C_o} \tag{2}$$

where C_0 and C_t represent concentrations of dye at time 0 min and t(s), respectively.

Anti bacterial assay using well diffusion method

The CdS nanoparticles were tested for antimicrobial activity using agar well diffusion method against pathogenic microbes such as *Acinetobacter baumannii, S. aureus,* and *E. coli.* The pure cultures of bacteria were subcultured on nutrient broth. Each strain was swapped homogeneously onto the individual plates using sterile cotton swabs. Wells of 8 mm were made on the nutrient agar plates. Then 25 μL, 50 μL, 75 μL and 100 μL concentration of CdS nanoparticles was poured on each well. Zone of inhibition was measured after 24 hours' incubation.

Haemolysis

CdS nanoparticles having concentration of 2 mg/mL, 4 mg/mL, 6 mg/mL, 8 mg/mL and 10 mg/mL and 1 mL erythrocyte/phosphate buffered saline (PBS) suspension (1×10^6 cells per mL) were incubated for 1 h at 37 °C. This was followed by centrifugation at 2,000 rpm for 10 min. The degree of haemolysis was determined by measuring the absorbance of the supernatant at 545 nm, as previously reported. Triton X-100 was used as positive control while blood/PBS solution was used as negative.

RESULTS AND DISCUSSION

UV-visible studies

Using UV-Vis spectrophotometer CdS NPs showed maximum absorbance at 496 nm as shown in Figure 1(a) and the band gap was calculated using Tauc plot given in Equation (3).

$$(\alpha h\upsilon)^{1/n} = \beta(h\upsilon - Eg) \tag{3}$$

where 'α' represents the absorption coefficient, '$h\upsilon$' is the photon energy, ' Eg' is the band gap and value of 'n' depends on transition involved, where n can have values 2, 1/2, 3, 3/2 related to indirect allowed, direct allowed, indirect forbidden and direct forbidden transitions, respectively. CdS nanoparticles show direct allowed transitions (Imran *et al.* 2018). To calculate the value of band gap, graph was plotted between $(\alpha h\upsilon)^2$ and $h\upsilon$, and the straight line obtained was extrapolated to zero absorption co-efficient so that it encountered the x-axis. The band gap of CdS was found to be 2.38 eV (Figure 1(b)).

XRD studies

X-ray diffraction powder analysis was carried out to investigate the crystallinity, crystallite size, and phase of nanoparticles. There is no extra peak, which indicates the purity of the synthesized NPs (Devendran *et al.* 2013). XRD pattern shown in Figure 1(c) indicated hexagonal pattern of CdS NPs. The diffraction peaks were observed at 24.840°, 26.370°, 30.47°, 43.79°, 51.87°, 54.32°, 63.62°, 70.17°, and 72.36° at 2θ and indexed to be characteristic 100, 002, 101, 102, 110, 103, 112 and 211, respectively, for CdS NPs, similar to JCPDS card no # 00-041-1049.

FTIR studies

FTIR spectroscopy was used to confirm the purity and to investigate the functional groups of precursors or any other impurities. FTIR spectra were obtained in the range of 500–4,000 cm^{-1}. In Figure 1(d), the peak at 400–700 cm^{-1} corresponds to the metal-sulphur bond. The peak at 630.33 cm^{-1} corresponds to Cd-S bonding mode and reveals the formation of CdS nanoparticles. The broad peak observed at 3,350.67 cm^{-1} was assigned to O-H (hydroxyl group) present because of the moisture absorbed by the CdS NPs. Symmetric C ≡ C bond mode was observed at 2,110.32 cm^{-1}, and a peak at 1,633.54 cm^{-1} was due to asymmetric stretching of C = C bond representing the presence of traces of organic impurities (Mahdi *et al.* 2017).

SEM and EDX studies

The SEM image shown in Figure 2(a) obtained with 500 nm magnification indicates the formation and shape (morphology) of nanoparticles. The grains of particles have been aggregated to form clusters. EDX analysis was performed for finding the

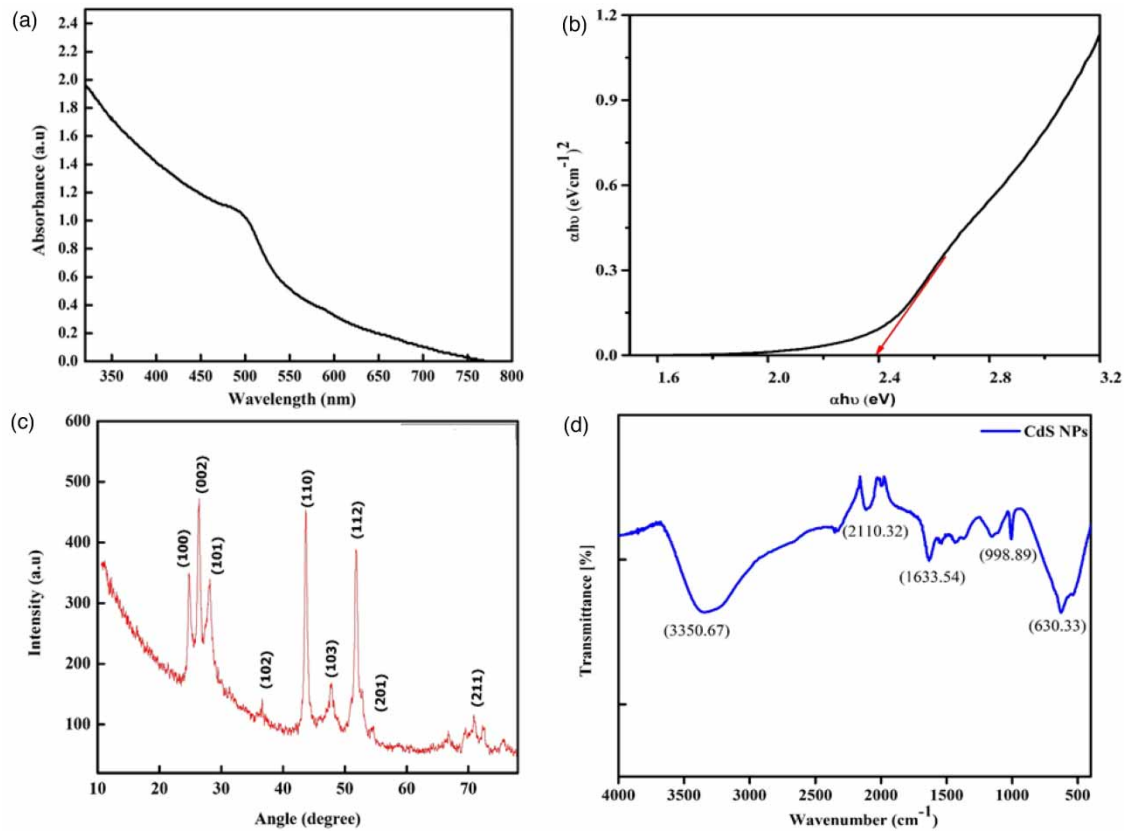

Figure 1 | (a) UV-Vis spectrum (b) Band gap (c) XRD pattern and (d) FTIR spectrum of CdS nanoparticles.

elemental composition of CdS NPs as shown in Figure 2(b). The EDX spectra reveal the presence of Cd and S as major elements in synthetic material and provide the quantitative analysis of weight percentage of compositional elements.

Thermo gravimetric analysis (TGA) of CdS nanoparticles

TGA was used to study thermal behavior of the prepared CdS NPs. The utility of these NPs for various applications depends upon temperature and temperature-induced phase changes (Ayodhya & Veerabhadram 2019). The TGA was carried out under N_2 atmosphere in the temperature range of 25–600 °C at a heating rate of 10 °C/min. The TGA curve of the sample shown in Figure 2(c) and 2(d) exhibited that the sample was quite stable to temperature. The weight loss of CdS was 4.89% from 40 to 250 °C, which is due to the presence of water and moisture content present in sample. The weight loss after 250 °C can mainly be assigned to the degradation of the nanomaterials and was only 1.65%. The TGA study indicated that the synthesized CdS nanomaterials were very stable to temperature and the total loss occurring was 6.54% only at 25 °C–600 °C.

Kinetics analysis

The kinetics of CdS catalyzed degradation of EB and MG dyes can be designated by Eley-Rideal (E-R) mechanism. According to this mechanism, oxygen molecules attack on the surface of catalyst in adsorbed form with the molecule of dye in fluid form (Ilyas & Saeed 2010). It has been examined that an electron-hole pair is formed between VB and CB of CdS nanocatalyst. Adsorbed oxygen present at the surface of CdS NPs takes up the electron and results in superoxide anion (O_2^-) formation. The proton produced from superoxide anion generates energetic OH radicals. The hole created in VB of CdS moves towards the exterior, where it combines with a molecule of water and generates active OH radicals. These active species play a important role in the photodegradation of EB and MG dyes. The E-R mechanism can be described in terms of kinetics expression as

$$\frac{-dC}{dt} = k_r C\theta_{O2} \tag{4}$$

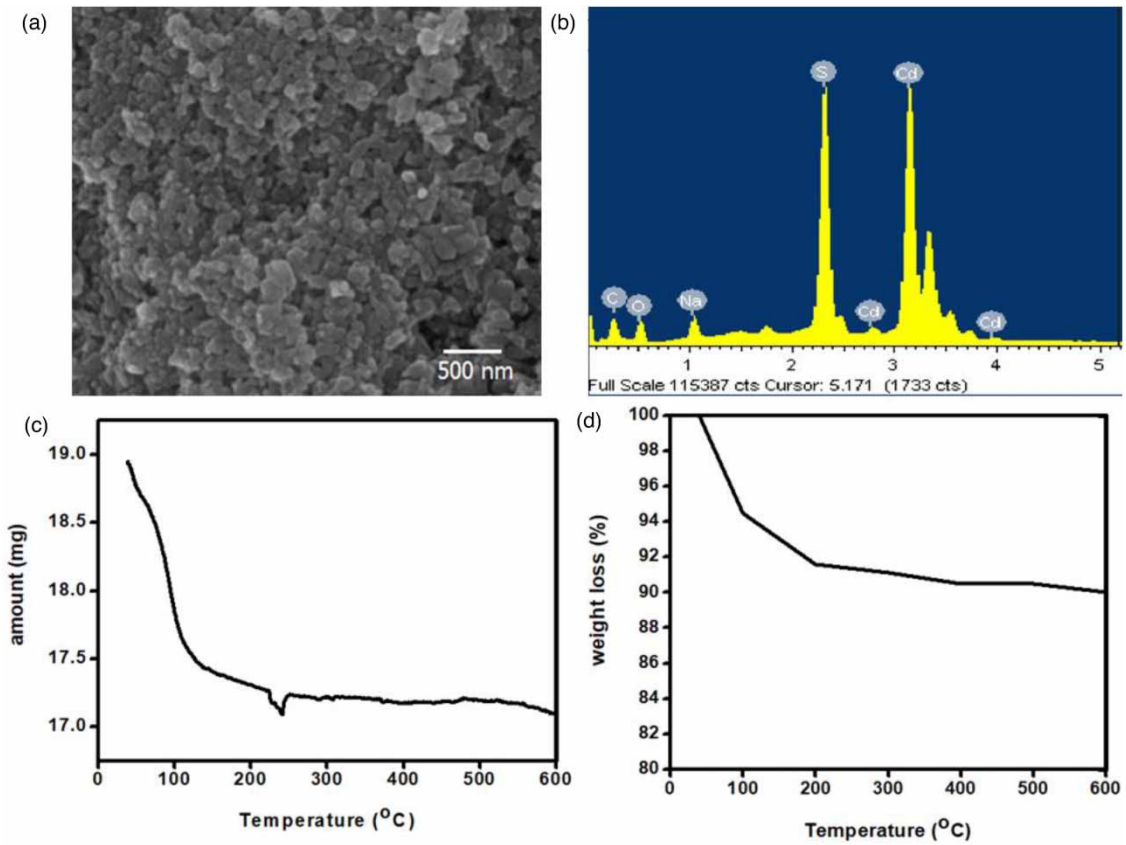

Figure 2 | (a) Scanning electron micrograph, (b) Energy dispersive X-rays spectrum, (c) TGA curve of CdS weight loss in mg and (d) weight loss in percentage of CdS NPs.

where as θ_{O2} and C represent concentration of EB and MG dye and concentration of oxygen at the surface respectively. By providing oxygen continuously make the reaction zero order with respect to oxygen, so expression of kinetic becomes as

$$\frac{dC}{dt} = k_{App}C \tag{5}$$

where k_{App} represents the rate constant of reaction and the above equation can be written in the integrated form as

$$\ln\left(\frac{Co}{C}\right) = k_{App} \cdot t \tag{6}$$

where as Co stands for initial concentration of dye and C for the concentration of dye after UV light illumination.

Equation (6) is realistic at various reaction temperatures (25 °C, 35 °C, 45 °C). The kinetic analysis for the photodegradation of EB and MG dyes as shown in Figure 3(a)–3(d) illustrates that the catalyst identity affects the speed of photocatalytic reaction. Tables 1 and 2 show the pseudo-first-order and pseudo-second-order photodegradation reaction parameters like k_{App} and their correlation coefficients. Kinetic parameters indicate how the catalytic performance is influenced by the interaction with CdS NPs. For the estimation of pseudo-second-order kinetics for the photodegradation of the EB and MG dye, the following mathematical expression was applied.

$$\frac{1}{C} - \frac{1}{Co} = k_{APP} \cdot t \tag{7}$$

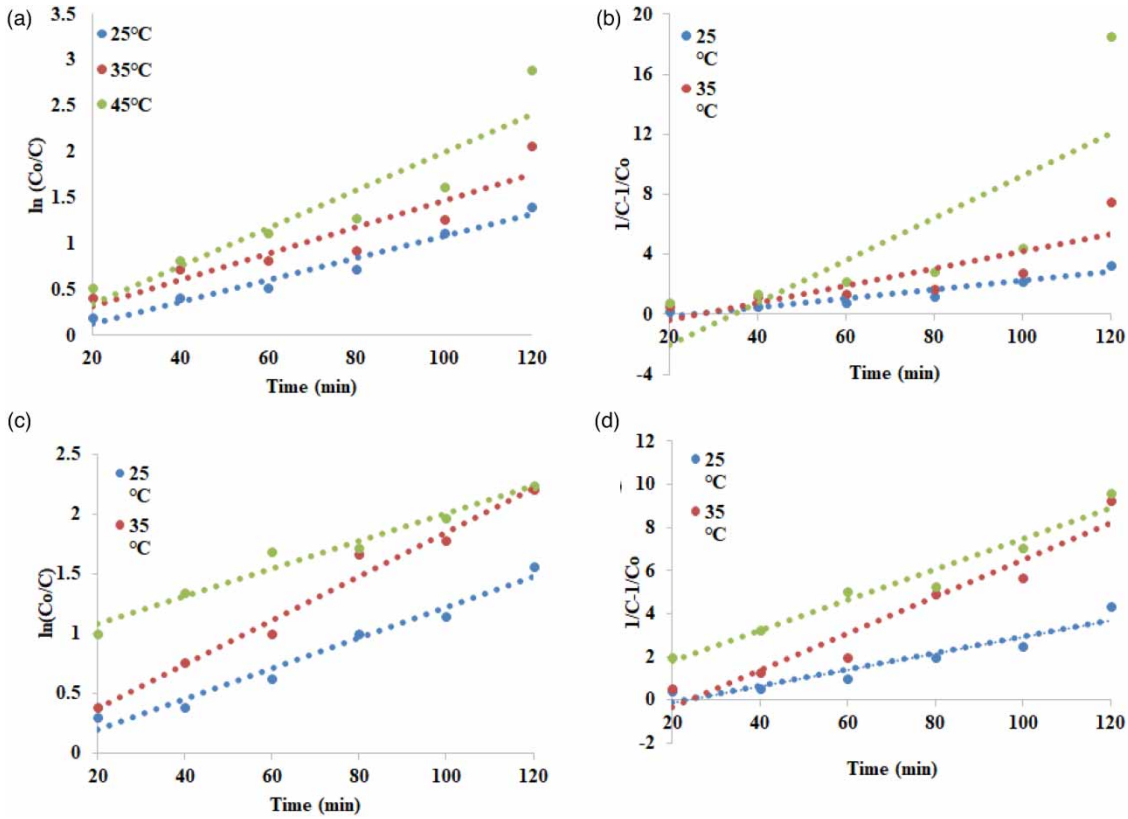

Figure 3 | (a) Application of pseudo-first-order kinetics, (b) pseudo-second-order kinetics to EB dye, (c) Application of pseudo-first-order kinetics and (d) pseudo-second-order kinetics to MG dye degradation using CdS NPs at various temperatures.

Table 1 | Kinetic constant parameter values for the photodegradation of EB dye at various temperatures

Temperature (Degree Celsius)		Pseudo-first-order kinetics		Pseudo-second-order kinetics		
		k_{App}	R^2	k_{App}	R^2	Activation Energy (kJ/mol)
CdS	25	0.0119	0.9672	0.0297	0.9954	61.1
	35	0.0144	0.8631	0.0573	0.6966	
	45	0.0206	0.8557	0.1409	0.8991	

Table 2 | Kinetic constant parameter values for the photodegradation of MG dye at various temperatures

Temperature (Degree Celsius)		Pseudo-first-order kinetics		Pseudo-second-order kinetics		
		k_{App}	R^2	k_{App}	R^2	Activation Energy (kJ/mol)
CdS	25	0.0129	0.9697	0.0379	0.9009	32.11
	35	0.0184	0.9786	0.0853	0.9296	
	45	0.0115	0.968	0.071	0.9592	

Tables 1 and 2 exhibited that the correlation coefficient along with their k_{App} of the pseudo-first- and second-order photo-degradation reaction of EB and MG dye over CdS NPs. However due to lower values obtain of K_{App} from pseudo-first-order, the data was best fitted to pseudo-second-order kinetics.

The Arrhenius equation was used to find out the activation energy of the given reaction and is given as

$$k = Ae\frac{-Ea}{RT} \tag{8}$$

where in Equation (8) the term Ea represents the activation energy and k represent rate constant of the reaction. The equation in logarithmic form is

$$\ln k = \ln A \quad -\frac{Ea}{RT} \tag{9}$$

Figure 4(a) and 4(b) represented that a straight line is obtain by interpreting a graph between lnk and 1/T with a negative slope Ea/R. The activation energy that was calculated from the slope of graph for the degradation of EB and MG was found to be 61.1 kJ/mol and 32.11 kJ/mol, as revealed in Tables 1 and 2.

The effect of concentration of the dyes on the rate of reaction using 0.03 g of CdS as photocatalyst was also studied. Different concentrations i.e. 10, 15, 25 and 35 mg L^{-1}, of dyes were used. The experimental data was evaluated on first-order and second-order rate constant equations as shown in Figure 5(a)–5(c), to obtain the apparent rate constant and correlation coefficient values. Tables 3 and 4 depict the values of apparent rate constants along with their respective regression coefficients.

All the parameters indicated that the data best fitted pseudo second-order kinetics.

Mechanism of photocatalytic degradation of Methylene Blue dye

Photocatalysis usually involves photo-absorption and photo-excitation of electrons from VB to the CB of a semiconductor material as shown in Figure 6. Electron–hole formation (Equation (10)), their transfer across the valence, conduction and forbidden energy bands and their recombination have been reported in the photocatalysis on the basis of band gap theory. Upon absorption of a higher-energy photon, an electron is promoted from the VB to the CB (e^-) of CdS with simultaneous generation of a hole (h^+) in the VB. The electrons and holes recombine in the bulk or surface of the particle in a few nanoseconds.Trapped energy in the surface sites can react with donor (D) or acceptor (A) species adsorbed or close to the surface of the particle. $OH^{\cdot -}$ radicals are generated when a h^+ in VB reacts with a water molecule (Equation (11)) and O_2^- radicals are formed by the reaction of an electron in CB with a dissolved O_2 molecule (Equation (12)). Complete

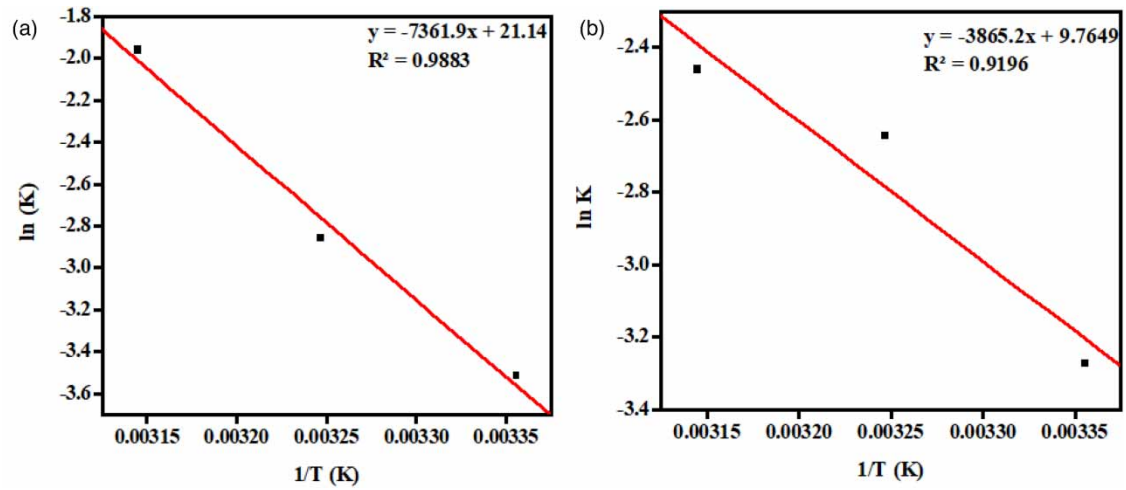

Figure 4 | Application of Arrhenius equation to (a) EB and (b) MG dye degradation using CdS NPs.

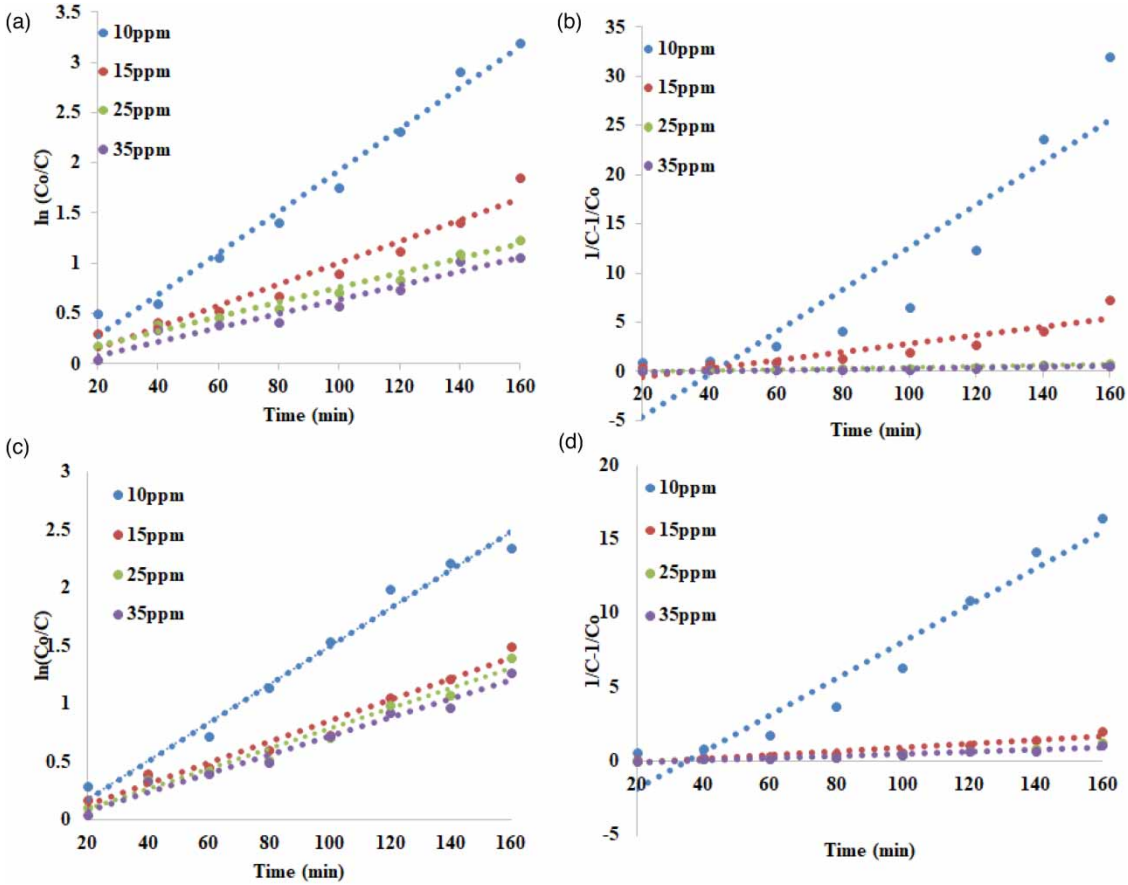

Figure 5 | (a) Application of pseudo-first-order kinetics (b) pseudo-second-order kinetics to EB dye, (c) Application of pseudo-first-order kinetics and (d) pseudo-second-order kinetics to MG dye degradation using CdS NPs at various initial concentrations.

Table 3 | At different initial concentrations, kinetic constant parameter values for the photocatalytic degradation of EB dye

		Pseudo-first-order kinetics		Pseudo-second-order kinetics	
Concentration (ppm)		k_{App}	R^2	k_{App}	R^2
CdS	10	0.0206	0.982	0.2154	0.8325
	15	0.0106	0.9457	0.0424	0.8102
	25	0.0072	0.9793	0.0055	0.9307
	35	0.007	0.9507	0.0039	0.9195

Table 4 | At different initial concentrations, kinetic constant parameter values for the photocatalytic degradation of MG dye

		Pseudo-first-order kinetics		Pseudo-second-order kinetics	
Concentration (ppm)		k_{App}	R^2	k_{App}	R^2
CdS	10	0.0165	0.9805	0.1235	0.9395
	15	0.0091	0.9724	0.0131	0.8994
	25	0.0087	0.9725	0.0071	0.934
	35	0.0081	0.9783	0.0082	0.9014

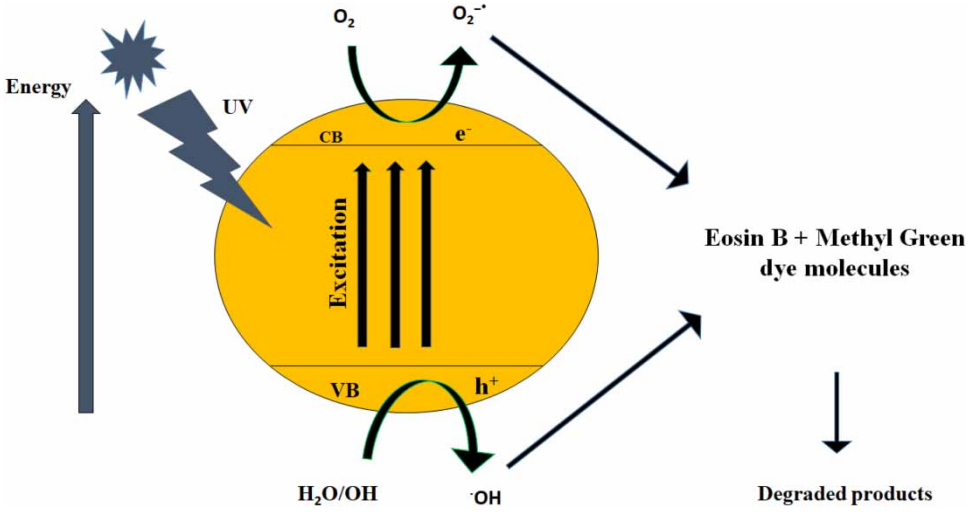

Figure 6 | Mechanism of possible photocatalytic degradation of EB and Mg dye by using CdS NPs.

conversion of an organic substrate to CO_2 and H_2O is carried out by the oxidative pathway (Faisal *et al.* 2021).

$$CdS + h\nu(\text{light}) \rightarrow e^- + h^+ \quad (10)$$

$$h^+ + H_2O \rightarrow {}^{\cdot}OH + H^+ \quad (11)$$

$$e^- + O_2 \rightarrow {}^{\cdot}O_2^- \quad (12)$$

$${}^{\cdot}OH + \text{dye molecules} \rightarrow \text{degraded products}$$

$$O_2^{\cdot-} + \text{dye molecules} \rightarrow \text{degraded products}$$

Factors affecting the degradation of dyes

Effect of time and concentration

The effect of irradiation time and initial dye concentration on the photocatalytic degradation of EB and MG with different initial dye concentration, i.e. 10, 15, 25 and 35 ppm, was evaluated by varying irradiation time. From Figure 7(a) and 7(b)

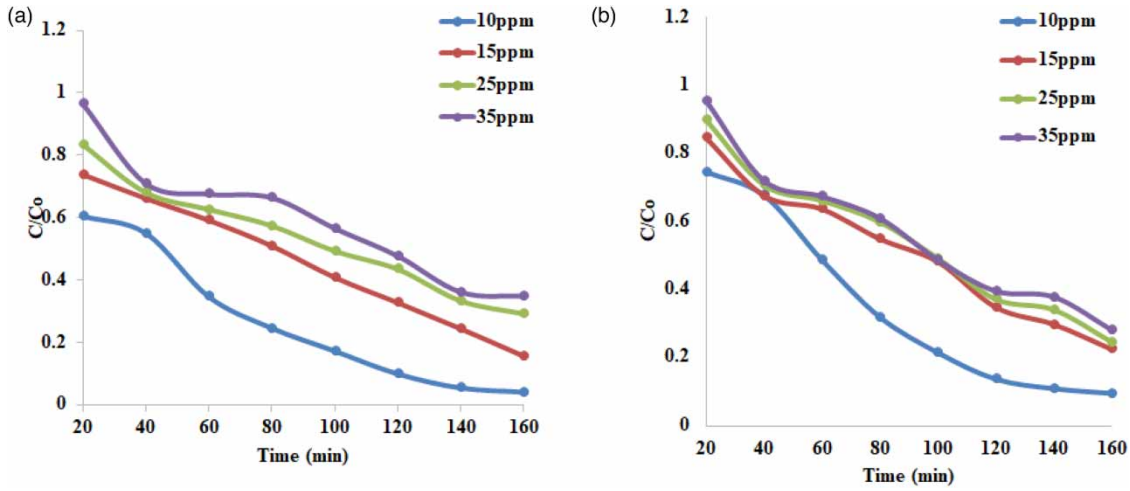

Figure 7 | Effect of concentration on the degradation of (a) EB and (b) MG dye.

it is evident that by increasing the initial concentration from 10 to 35 ppm, the percent degradation decreased from 95% to 65% and from 90% to 71% for EB and MG, respectively. Duration of irradiation directly affects the interaction between photons and photocatalysts. Greater contact is achieved at longer irradiation time, and consequently more OH radicals are produced (Jan *et al.* 2021). Due to the greater availability of active sites on the surface of the photocatalyst at lower dye concentrations, higher percent degradation can be observed. The degradation rate was found to decrease as the initial dye concentration was increased. This can be explained by the fact that increasing the dye concentrations reduces the amount of light that reaches the organic molecules of both colours (Kokilavani *et al.* 2021).

Effect of temperature

The temperature effect on EB and MG dyes degradation using 10 ppm concentration of dyes at the time duration of 120 minutes in aqueous solutions in the presence of CdS was studied at various temperatures, i.e. 25, 35 and 45 °C, as shown in Figure 8(a) and 8(b). An increase in percent degradation of dye was observed through increase in temperature. Maximum degradation (94.4%) was observed for EB dye and 89.2% for MG dye at 45 °C in 120 minutes, respectively. The degradation of dyes increased as the temperature was increased. This is due to the fact that at high temperatures, the interaction of dye molecules with the photocatalyst surface increases, favouring dye photodegradation (Kumar & Pandey 2017).

Effects of catalyst dosage

The effect of catalyst dosage on EB and MG degradation was investigated by changing the catalyst's mass from 0.01 g/L to 0.05 g/L with illumination under UV light for 140 minutes as shown in Table 5 and supplementary Figures 2 and 3. An increase in dye degradation was observed with an increase in CdS photocatalyst mass from 0.01 g/L to 0.03 g/L. This can be attributed to the fact that an increase in catalyst mass possibly contributes an increased surface, resulting in more photons received at the surface of the catalyst (Christopher *et al.* 2011). Shielding of the photons by the suspension also occurs at increased catalyst dosage. An optimum amount of catalyst should be used for dye degradation in wastewater, above which the rate of degradation will eventually decrease. Maximum catalyst dosage for maximum activity has been reported to be 3–4 g/L of dye solution (Mohammadzadeh *et al.* 2015).

Effect of pH

Degradation of the dyes is strongly affected by the pH of the medium, as the ionization of the surface functional groups is influenced by the solution pH. The effect of pH on the degradation of EB and MG was studied by varying the pH from 4 to 10. As is evident from Table 6 and supplementary Figure 4, with increase in pH, degradation ability of EB also increased. This can be attributed to the fact that at high pH a greater number of the negatively charged sites are available on the adsorbent surface. Strong electrostatic attraction between the cationic dye (EB) and OH ions present in the catalyst leads to utmost degradation of dyes from the medium (NirmalaDevi *et al.* 2018).

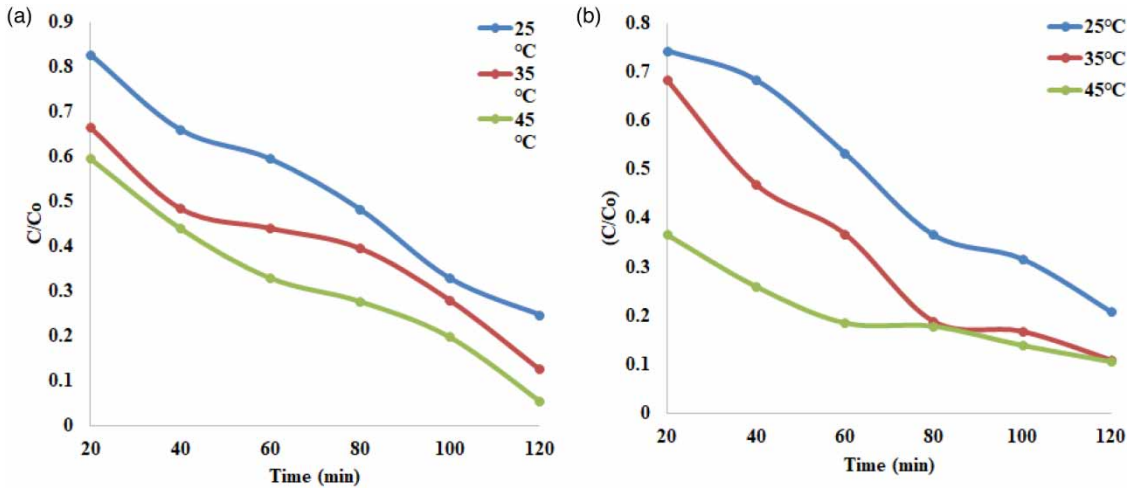

Figure 8 | Effect of temperature on degradation of (a) EB and (b) MG dye.

Table 5 | Percent degradation of EB dye and MG dye using different dosage of CdS NPs

Catalyst dosage (g/L)	0.01	0.02	0.03	0.04	0.05
Eosin B (%) degradation	48	55.8	61.5	54.1	49.6
Methyl Green (%) degradation	43	74.4	81.7	56.4	50.9

Table 6 | Percent degradation of CdS NPs on EB dye and MG dye degradation at different pH

pH	4	5	6	7	8	9	10
Eosin B (%) degradation	33.1	43.4	47.3	62.5	64.9	77.9	79.2
Methyl Green (%) degradation	88.3	67.8	62.8	53.1	43.4	38.7	35.4

Conversely, MG is anionic dye and behaves differently as compared to EB dye. Maximum degradation was observed at low pH (pH = 4). This can be attributed to the fact that a larger amount of MG can adsorb on the catalyst surface at low solution pH, as evident from Table 6 and supplementary Figure 5. The adsorption of anionic adsorbate species on the negatively charged surfaces of the catalyst is opposed at higher pH. The surface tends to acquire positive charge at low pH, thereby resulting in an increased adsorption of dyes, thus increasing electrostatic attraction between the negatively charged dye and the positively charged catalyst (Haque *et al.* 2011). Our results are in agreement with previously reported results.

Effect of reusability of catalyst

The reusability of photocatalyst is important in large-scale processes; that's why the recyclability and stability of the CdS photocatalyst was investigated through the degradation of EB and MG dye under UV light illumination. The catalyst was centrifuged and then recycled without further treatment by washing with ethanol, twice deionized water, and drying at 50 °C for 30 minutes. The maximum photocatalytic efficiency of CdS for EB was 65.3% and for MG dye was 64.4% in 140 minutes' time interval, as shown in Table 7 and supplementary Figures 6 and 7 respectively. From the figure it is evident that a slight decline in the recovery occurs as compared to the original. This can be explained by the catalyst's excellent stability and durability, as evidenced by its low loss and deactivation during the cycling experiment (Chen *et al.* 2017).

Antibacterial activity by well diffusion method

Figure 9 displays antibacterial activity of CdS nanoparticles. Pathogenic bacterial strains such as *A. baumannii, S. aureus* and *E. coli* were used for this study. The results showed that chemically synthesized CdS were energetically involved in the antibacterial activity against pathogenic bacteria. Good antibacterial activity against *S. aureus* was shown by CdS NPs. It can be explained that CdS NPs might have better penetration through the agar and consequently into cell bacteria than the plant extract due to the small size of nanoparticles. Hypothetical theories reveal that the inhibition is caused by ionic adsorption of nanoparticles on the bacteria's surface, resulting in a high intensity of the proton motive force. However, the actual mechanism of the bacteria's inhibition is yet unknown. One idea claims that NPs infiltrate the bacterial cell and bind to essential enzymes containing thiol groups (Prasad & Swamy 2013).

Human RBC haemolysis assay

Table 8 and supplementary Figure 8 depict the degree of haemolysis caused by CdS nanoparticles exposed to human red blood cells for 1 h of incubation. With increase in the concentration of nanoparticles in the PBS/RBC mixture, the percent

Table 7 | Percent degradation of CdS NPs at recovered catalyst on EB dye and MG dye degradation

Time (min)	20	40	60	80	100	120	140
Re-used CdS Eosin B (%) degradation	25.5	35.3	39.4	42.2	50.5	58.8	65.3
Re-used CdS Methyl Green (%) degradation	14.4	16.1	35.7	51.3	56.5	59.3	64.4

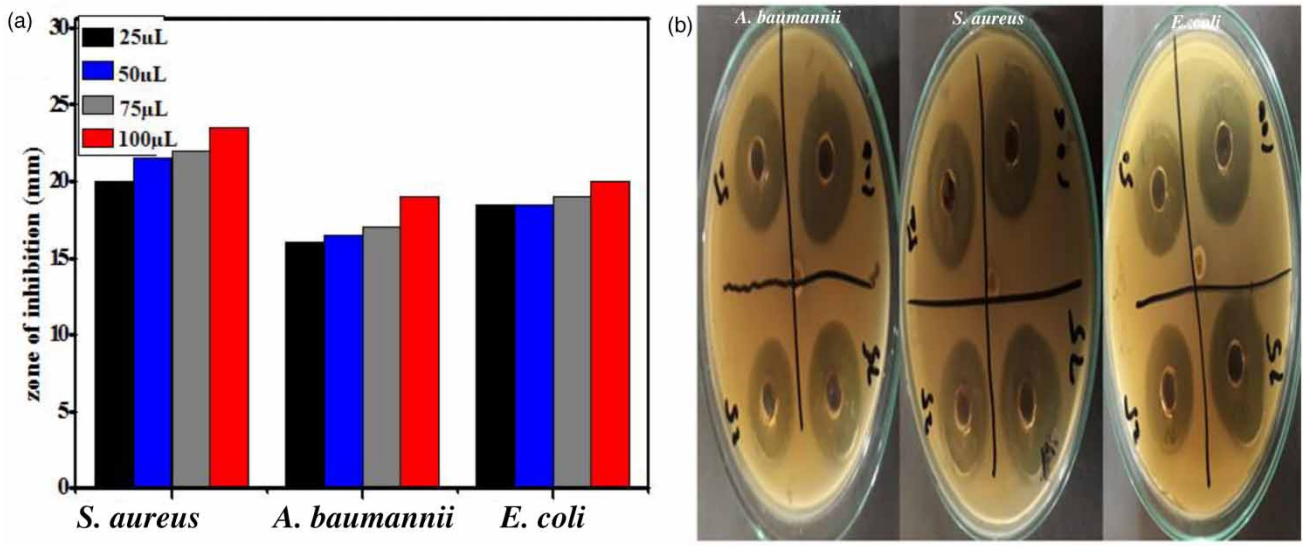

Figure 9 | (a) and (b) Anti-bacterial activity of CdS NPs.

Table 8 | Biocompatibility study of CdS NPs

Concentration of CdS NPs	PBS	2 mg/mL	4 mg/mL	6 mg/mL	8 mg/mL	10 mg/mL	Triton X-100
Hemolysis (%)	1.00	29.17	35.40	48.30	62.30	77.70	99.54

haemolysis also increased. For the particle concentrations at 2 mg/mL, CdS NPs caused significantly greater levels of haemolysis, exceeding 29%. The ASTM E2524–08 standard criterion states that haemolysis of more than 5% indicates that the test material damages RBCs, but this criterion was exceeded in the pour study at a particle concentration of 2 mg/mL for CdS nanoparticles. Because 5% haemolysis is considered a permissible limit for nanomaterials, up to 2 mg/mL of CdS nanoparticles can be used for haemolysis activity. As a result, the generated CdS nanoparticles can be said to be biocompatible in nature at very low concentrations (Singh *et al.* 2019).

CONCLUSION

The CdS successfully synthesized through the hydrothermal route have a band gap of 2.38 eV. The particles were aggregated to form clusters with crystalline hexagonal structures. CdS nanoparticles were found to be very stable to temperature as a small loss (6.54%) in weight occurred during heating from 25 °C to 600 °C. More than 89% dye degradation was noticed at 160 minutes' time duration for both the dyes. The dye degradation was found to decrease with increase in the initial concentration of dyes. Increasing the temperature enhanced % degradation, while with varying pH the dyes behaved differently. High % degradation of EB was observed at high pH (pH 10), while at low pH (pH 4) high % degradation was found for MG dye. Up to pH 9 of the medium the degradation was found to increase. The degradation of EB and MG over CdS catalyst surface follows second-order kinetics. The recyclability study showed that the CdS are stable and durable nanoparticles. At lower concentration, CdS NPs are found to be biocompatible, while good antibacterial activity was shown against *S. aureus*.

DATA AVAILABILITY STATEMENT

All relevant data are included in the paper or its Supplementary Information.

REFERENCES

Ayodhya, D. & Veerabhadram, G. 2019 Facile fabrication, characterization and efficient photocatalytic activity of surfactant free ZnS, CdS and CuS nanoparticles. *Journal of Science: Advanced Materials and Devices* **4** (3), 381–391.

Blažeka, D., Car, J., Klobučar, N., Jurov, A., Zavašnik, J., Jagodar, A. & Krstulović, N. 2020 Photodegradation of Methylene Blue and Rhodamine B using laser-synthesized ZnO nanoparticles. *Materials* **13** (19), 4357.

Chang, Z., Zhang, J., Dong, W., Meng, X., Wang, H., Wei, D. & Ren, Y. 2020 Cadmium sulfide net framework nanoparticles for photo-catalyzed cell redox. *RSC Advances* **10** (62), 37820–37825.

Chen, X., Wu, Z., Liu, D. & Gao, Z. 2017 Preparation of ZnO photocatalyst for the efficient and rapid photocatalytic degradation of azo dyes. *Nanoscale Research Letters* **12** (1), 1–10.

Christopher, P., Xin, H. & Linic, S. 2011 Visible-light-enhanced catalytic oxidation reactions on plasmonic silver nanostructures. *Nature Chemistry* **3** (6), 467–472.

Desai, K. R., Pathan, A. A. & Bhasin, C. P. 2017 Synthesis, characterization of cadmium sulphide nanoparticles and its application as photocatalytic degradation of congored. *International Journal of Nanomaterials and Chemistry* **3**, 39.

Devendran, P., Alagesan, T. & Pandian, K. 2013 Single pot microwave synthesis of CdS nanoparticles in ionic liquid and their photocatalytic application. *Asian Journal of Chemistry* **25** (Supplementary Issue), S79.

Faisal, S., Jan, H., Shah, S. A., Shah, S., Khan, A., Akbar, M. T. & Syed, S. 2021 Green synthesis of zinc oxide (ZnO) nanoparticles using aqueous fruit extracts of *Myristica fragrans*: their characterizations and biological and environmental applications. *ACS Omega* **6** (14), 9709–9722.

Haque, E., Jun, J. W. & Jhung, S. H. 2011 Adsorptive removal of methyl orange and methylene blue from aqueous solution with a metal-organic framework material, iron terephthalate (MOF-235). *Journal of Hazardous Materials* **185** (1), 507–511.

Ilyas, M. & Saeed, M. 2010 Oxidation of benzyl alcohol in liquid phase catalyzed by cobalt oxide. *International Journal of Chemical Reactor Engineering* **8** (1), https://doi.org/10.2202/1542-6580.2162.

Imran, M., Ikram, M., Shahzadi, A., Dilpazir, S., Khan, H., Shahzadi, I. & Huang, Y. 2018 High-performance solution-based CdS-conjugated hybrid polymer solar cells. *RSC Advances* **8** (32), 18051–18058.

Jan, F. A., Ullah, R., Ullah, N. & Usman, M. 2021 Exploring the environmental and potential therapeutic applications of *Myrtus communis* L. assisted synthesized zinc oxide (ZnO) and iron doped zinc oxide (Fe-ZnO) nanoparticles. *Journal of Saudi Chemical Society* **25** (7), 101278.

Kokilavani, S., Syed, A., Rajeshwari, M. R., Subhiksha, V., Elgorban, A. M., Bahkali, A. H. & Khan, S. S. 2021 Decoration of Ag_2WO_4 on plate-like MnS for mitigating the charge recombination and tuned bandgap for enhanced white light photocatalysis and antibacterial applications. *Journal of Alloys and Compounds* **889**, 161662.

Kumar, A. & Pandey, G. 2017 A review on the factors affecting the photocatalytic degradation of hazardous materials. *Material Science & Engineering International Journal* **1** (3), 1–10.

Lee, S. Y., Kang, D., Jeong, S., Do, H. T. & Kim, J. H. 2020 Photocatalytic degradation of rhodamine B dye by TiO_2 and gold nanoparticles supported on a floating porous polydimethylsiloxane sponge under ultraviolet and visible light irradiation. *ACS Omega* **5** (8), 4233–4241.

Mahdi, H. S., Parveen, A., Agrawal, S. & Azam, A. 2017 Microstructural and optical properties of sol gel synthesized CdS nano particles using CTAB as a surfactant. In: *AIP Conference Proceedings*. AIP Publishing LLC. Vol. 1832, No. 1, p. 050012.

Menon, S., Agarwal, H. & Shanmugam, V. K. 2021 Catalytical degradation of industrial dyes using biosynthesized selenium nanoparticles and evaluating its antimicrobial activities. *Sustainable Environment Research* **31** (1), 1–12.

Mohammadzadeh, S., Olya, M. E., Arabi, A. M., Shariati, A. & Nikou, M. K. 2015 Synthesis, characterization and application of ZnO-Ag as a nanophotocatalyst for organic compounds degradation, mechanism and economic study. *Journal of Environmental Sciences* **35**, 194–207.

Mullamuri, B., Mosali, V. S. S., Maseed, H., Majety, S. S. & Chandu, B. 2021 Photocatalytic activity of heavy metal doped CdS nanoparticles synthesized by using Ocimum sanctum leaf extract. *Bio Interface Research in Applied Chemistry* **11** (5), 12547–12559.

Munyai, S., Tetana, Z. N., Mathipa, M. M., Ntsendwana, B. & Hintsho-Mbita, N. C. 2021 Green synthesis of Cadmium Sulphide nanoparticles for the photodegradation of Malachite green dye, Sulfisoxazole and removal of bacteria. *Optik* **247**, 167851.

NirmalaDevi, V., Makeswari, M. & Santhi, T. 2018 Malachite Green dye degradation using $ZnCl_2$ activated *Ricinus communis* stem by sunlight irradiation. *Rasāyan Journal of Chemistry* **11** (1), 219–227.

Prasad, R. & Swamy, V. S. 2013 Antibacterial activity of silver nanoparticles synthesized by bark extract of *Syzygium cumini*. *Journal of Nanoparticles* **2013**, 1–6.

Rajeshkumar, S., Ponnanikajamideen, M., Malarkodi, C., Malini, M. & Annadurai, G. 2014 Microbe-mediated synthesis of antimicrobial semiconductor nanoparticles by marine bacteria. *Journal of Nanostructure in Chemistry* **4** (2), 96.

Sarkar, S., Ponce, N. T., Banerjee, A., Bandopadhyay, R., Rajendran, S. & Lichtfouse, E. 2020 Green polymeric nanomaterials for the photocatalytic degradation of dyes: a review. *Environmental Chemistry Letters* **18**, 1–12.

Singh, V., Rao, A., Tiwari, A., Yashwanth, P., Lal, M., Dubey, U. & Roy, B. 2019 Study on the effects of Cl and F doping in TiO_2 powder synthesized by a sol-gel route for biomedical applications. *Journal of Physics and Chemistry of Solids* **134**, 262–272.

First received 12 October 2021; accepted in revised form 14 December 2021. Available online 20 January 2022